Eur. J. Mineral.
2002, **14**, 1129–1138

# Interlayer vacancy characterization of synthetic phlogopitic micas by IR spectroscopy

BERND WUNDER* and STEFAN MELZER

GeoForschungsZentrum Potsdam, Div. 4, Telegrafenberg, D-14473 Potsdam, Germany
* Corresponding author, e-mail: wunder@gfz-potsdam.de

**Abstract:** Phlogopitic micas of the solid solution binaries $KMg_3[AlSi_3O_{10}](OH)_2$ (phlogopite) – $RbMg_3[AlSi_3O_{10}](OH)_2$ (Rb-phlogopite), phlogopite – $CsMg_3[AlSi_3O_{10}](OH)_2$ (Cs-phlogopite), and phlogopite – $BaMg_3[Al_2Si_2O_{10}](OH)_2$ (kinoshitalite) have been synthesized at temperatures of 700 and 800°C and pressures of 0.2 and 2.0 GPa. The run products have been investigated by optical microscopy, X-ray powder diffraction, electron microprobe, and infrared spectroscopy. All runs yielded between 81 and 100 wt.% of phlogopitic micas, beside traces of quartz, sanidine, and in one run talc. Celsian and cymrite formed as additional phases in the runs of the (K-Ba)-series. The synthetic phlogopitic micas often consist of mixtures of the three polytypes 1M, $2M_1$ and $2M_2$, with 1M being the most abundant polytype. Based on electron microprobe analyses, interlayer vacancy concentrations of up to 0.29 (p.f.u.) were determined, indicating a significant talc component within the synthesized phlogopitic micas. In addition to the known characteristic phlogopite OH-stretching vibrational bands, the infrared spectra of the synthetic micas with incompletely filled interlayer sites exhibit a further OH-band, centered in the spectral range 3674 – 3678 $cm^{-1}$. The intensity of this band is correlated with the amount of vacancies. The vacancy concentration of phlogopitic micas was determined quantitatively from the intensity of this infrared band by using the intensity of the principal OH-band of synthetic talc ($Mg_3[Si_4O_{10}](OH)_2$) as a standard. The vacancy concentration of the interlayer site as determined in such a way by infrared spectroscopy corresponds to those independently derived by electron microprobe analyses.

**Key-words:** phlogopitic micas, interlayer vacancies, IR spectroscopy.

## Introduction

Phlogopitic micas have been extensively investigated by numerous authors using infrared (IR) spectroscopy (*e.g.,* Vedder, 1964; Farmer, 1974; Tateyama *et al.,* 1976; Velde, 1983; Robert & Kodama, 1988). The various absorption bands in the OH-stretching vibrational region (3200 – 3800 $cm^{-1}$) are attributed to the specific atomic groupening at the octahedral, tetrahedral, and interlayer sites around the OH-sites. The principal and strongest OH-stretching frequency of phlogopite lies at about 3724 $cm^{-1}$. This band is called N-(normal) frequency after Vedder (1964) and represents hydroxyls, for which the neighboring octahedral sites are filled with divalent ions. For phlogopite, the ideal local octahedral coordination around a hydroxyl group leading to the N-band is $(MgMgMg)^{VI}$. The position of the N-band can slightly vary with the substitutions in the twelve-fold interlayer position and in the octahedral and tetrahedral sheets. In principle, the N-band of natural phlogopitic micas is rather broad (full widths at half maximum (FWHM) of about 25 $cm^{-1}$) representing the structural pertubations associated with the various interlayer, octahedral and tetrahedral substitutions (Farmer, 1974). According to *e.g*., Robert & Kodama (1988), OH-stetching bands lying in the frequency-range 3630 – 3675 $cm^{-1}$ are attributed to $Al^{3+}$-incorporation in the octahedral sheets replacing divalent cations. Generally, OH-vibrations resulting from the substitution of divalent ions by trivalent ions in the octahedral sites plus the additional processes required for neutrality (*e.g.,* $Al^{IV}$ for $Si^{IV}$) are named I- (impurity) bands after Vedder (1964). The local octahedral coordination can be described as $(MgAlMg)^{VI}$. The OH-stretching band system in the low-energy spectral range 3450 – 3620 $cm^{-1}$ is assigned to vacancies in the octahedral sheet ($\square^{VI}$), and are named V- (vacancy) bands after Vedder (1964). Processes required for neutrality are the substitution of two divalent ions in the octahedral sites by $Al^{3+}$ leading to $(Al\square Al)^{VI}$ as the local octahedral cation coordination around the hydroxyl group. For dioctahedral micas, Bresson & Drits (1997) showed that twelve-fold vacancies ($\square^{XII}$), which can be described as pyrophyllite-like local structural environments, cause an additional OH-band at about 3675 $cm^{-1}$. The energy of this band is in correspondance to the principal OH-stretching frequency of pyrophyllite. In analogy to dioctahedral micas, interlayer vacancies within phlogopitic micas can be chemically described as a talc component. Robert *et al.* (1983) observed for trioctahedral Li-mi-

0935-1221/02/0014-1129 $ 4.50
DOI: 10.1127/0935-1221/2002/0014-1129

cas an OH-frequency at 3678 $cm^{-1}$, which they attributed to vacant alkaline sites. In $NH_4$-phlogopite, Harlov *et al.* (2001) assigned an OH-stretching band at about 3675 $cm^{-1}$ to hydroxyls located in the vicinity of vacant interlayer sites. With the exception of these two studies, the influence of $\square^{XII}$ on the IR spectra of trioctahedral phlogopitic micas has not been considered up to now.

The present study was initiated by our recent investigations on synthetic (K,Rb,Cs)-phlogopitic micas (Melzer & Wunder, 2001), for which significant amounts of interlayer vacancies (up to 25 mole %) were determined by electron microprobe (EMP) analyses. However, the amount of interlayer vacancies was rather ambiguous due to a possible alkali-loss during EMP measurements. Therefore, aimed to find an accurate method for the characterization of the talc component within phlogopitic micas, in the present study we investigated a suite of well-defined synthetic (Cs, K, Rb, Ba)-phlogopites, exhibiting varying amounts of incompletely filled interlayer sites. We show that the OH-stretching band observed in the spectral range 3674 – 3678 $cm^{-1}$ of the synthetic samples by IR spectroscopy is due to the vacant interlayer site within phlogopite and that the intensity of this IR band can be correlated with the amount of the talc component, which was independently determined by EMP.

## Experimental and analytical methods

### Experimental methods

The runs are divided into three series. The first series is the $KMg_3[AlSi_3O_{10}](OH)_2$ (phlogopite) – $RbMg_3[AlSi_3O_{10}](OH)_2$ (Rb-phlogopite) series (K-Rb), the second one the phlogopite – $CsMg_3[AlSi_3O_{10}](OH)_2$ (Cs-phlogopite) series (K-Cs), and the third one the phlogopite – $BaMg_3[Al_2Si_2O_{10}](OH)_2$ (kinoshitalite) series (K-Ba). Run conditions were 800°C at 0.2 and 2.0 GPa; some synthesis experiments of the (K-Rb)-series were also performed at 700°C and 0.2 GPa. The run conditions of each experiment are summarized in Table 1.

For synthesis experiments at 0.2 GPa, standard cold-seal hydrothermal vessels were used. The temperature in the hydrothermal experiments was controlled internally by Ni-CrNi thermocouples next to the sample position. The uncertainty of the temperature is ±5°C. The pressure was measured with a calibrated strain-gauge. Pressure uncertainty of each run was less than 5 MPa. Runs lasted 10 to 14 days. The experiments were quenched by cooling the autoclaves with compressed air to less than 300°C in 3 minutes. High-pressure experiments at 2.0 GPa were conducted in a non-end-loaded piston-cylinder apparatus using NaCl-graphite-assemblies. Temperatures were measured using Ni-CrNi thermocouples with an accuracy of ±10°C. Pressure was calibrated using the equilibrium albite = jadeite + α-quartz. Uncertainties in pressure are approximately ±2 %. Runs lasted 5 to 7 days. The samples were quenched to 200°C in less than 15 seconds.

Mixtures of oxides of stoichiometric phlogopite composition with an excess of 5 wt.% $SiO_2$ were used as solid starting materials. The starting fluid was a 2 molal aqueous chloridic solution bearing either (K,Rb) for the first, (K,Cs) for the second, or (K,Ba) for the third series. Starting bulk compositions for the three series were chosen, such that solid solutions along the joins phlogopite – Rb-phlogopite, phlogopite – Cs-phlogopite and phlogopite – kinoshitalite were expected. The fluid/solid ratio was ≥ 2 for all syntheses experiments. Au-capsules of 25 mm length, 3 mm in diameter and wall-thickness of 0.3 mm for the experiments at 0.2 GPa and Pt-capsules of 10 mm length, 3 mm in diameter and 0.3 mm wall-thickness for the experiments at 2.0 GPa were used. The filled capsules were sealed using a plasma welder while cooled with an ice/water mixture. Further details of the experimental procedure for the synthesis of phlogopite of the (K,Rb)- and (K,Cs)-series have been described by Melzer & Wunder (2001).

### Analytical methods

Solid phases were characterized by optical microscopy, powder X-ray diffraction (XRD), EMP analyses and IR spectroscopy. Details of these methods are already described by Gottschalk & Andrut (1998) and are therefore only briefly documented herein.

XRD patterns were recorded in transmission using a fully automated STOE STADI P diffractometer (Cu$K\alpha_1$-radiation), equipped with a primary monochromator. Operating conditions were 40 kV and 40 mA. The spectra were recorded in the range of 5 to 125 °2θ using a step interval of 0.1°. The resolution of the PSD was set to 0.02°. Counting times were selected to yield a maximum intensity of 2000 to 3000 counts for each sample, resulting in 5 to 20 s per detector step. The unit cell and other structural parameters were refined using the *GSAS* software package for Rietveld refinement (Larson & Von Dreele, 1987). As initial structure models for the refinement of the various phlogopite polytypes, the structural parameter of Rayner (1974) for the *1M*-polytype, Bohlen *et al.* (1980) for the $2M_1$-polytype, and Sartori *et al.* (1973) for the $2M_2$-polytype were used.

EMP analyses were conducted with Cameca SX50 and SX100 microprobes equipped with wave-length dispersive systems and applyed PAP-correction (Pouchou & Pichoir, 1984). Operating conditions were 15 kV and 20 nA. Counting times for all elements were 20 s for the peak position and 10 s for the background. Well defined natural minerals were used as standards: for Si (wollastonite), for Mg (tremolite) and for K and Al (orthoclase). For Rb, Cs and Ba analyses, well characterized synthetic minerals were used. Rb was standardized on Rb-feldspar ($RbAlSi_3O_8$), Cs on pollucite ($CsAlSi_2O_6$) and Ba on celsian ($BaAl_2Si_2O_8$). EMP analyses of phlogopite were accepted if oxide sums were larger than 90 wt.%, except of run SM20-99 (see Table 2), where totals of about 89 – 90 wt.% were available.

For the IR absorption measurements, samples were prepared by grinding 1 mg of the run product and dispersing it into 450 mg of KBr. The homogenized mixtures were cold-pressed under vacuum to transparent pellets. Before recording the spectra, the pellets were dried at 170°C for 48 hours. IR absorption spectra were collected in the spectral range of 3400 to 3800 $cm^{-1}$ with a resolution of 0.25 $cm^{-1}$ using a

Table 1. Details of Rietveld refinement and derived phase proportions.

| run No. | SM 7-98 | SM 9-98 | SM 10-98 | SM 11-98 | SM 12-98 | SM 35-98 | SM 36-98 | SM 37-98 | SM 45-98 | SM 46-98 | SM 65-98 | SM 27-99 | SM 30-99 | SM 38-99 |
|---|---|---|---|---|---|---|---|---|---|---|---|---|---|---|
| temperature [°C] | 800 | 800 | 800 | 800 | 800 | 800 | 800 | 800 | 800 | 800 | 700 | 700 | 700 | 800 |
| pressure [MPa] | 200 | 200 | 200 | 200 | 200 | 2000 | 2000 | 200 | 2000 | 2000 | 200 | 200 | 200 | 200 |
| $X_K$(mica, see Table 2) | 0.31 | 0.70 | 0.73 | 0.36 | 0.72 | 0.65 | 0.51 | 0.00 | 0.33 | 0.24 | 0.48 | 0.71 | 0.65 | 0.25 |
| experimental series | **(K-Rb)-phlogopite series** | | | | | | | | | | | | | |
| refinement details | | | | | | | | | | | | | | |
| integrat.time/step interval [s] | 793 | 610 | 488 | 780 | 455 | 650 | 650 | 585 | 660 | 854 | 976 | 594 | 594 | 528 |
| max. counts/step | 3268 | 2347 | 2640 | 3113 | 2887 | 3152 | 3069 | 2649 | 2709 | 3136 | 2796 | 3428 | 3011 | 2820 |
| unique reflections | 3508 | 2461 | 2443 | 2525 | 1473 | 2460 | 2468 | 2646 | 2463 | 2454 | 2573 | 3164 | 3277 | 3575 |
| structural parameters | 73 | 76 | 77 | 76 | 26 | 79 | 79 | 73 | 78 | 76 | 75 | 63 | 75 | 54 |
| experimental parameters | 22 | 24 | 27 | 26 | 23 | 20 | 28 | 27 | 23 | 29 | 26 | 26 | 26 | 26 |
| *N-P* | 5897 | 5898 | 5894 | 5796 | 5347 | 5849 | 5941 | 5898 | 5897 | 5843 | 5847 | 5859 | 5847 | 5918 |
| *R* | 0.068 | 0.081 | 0.085 | 0.053 | 0.083 | 0.062 | 0.068 | 0.069 | 0.063 | 0.057 | 0.047 | 0.055 | 0.059 | 0.065 |
| Rwp | 0.091 | 0.107 | 0.112 | 0.073 | 0.108 | 0.085 | 0.091 | 0.093 | 0.084 | 0.075 | 0.062 | 0.075 | 0.078 | 0.087 |
| $\chi 2$ | 1.78 | 1.59 | 1.66 | 1.62 | 1.73 | 1.62 | 1.82 | 1.87 | 1.46 | 1.56 | 1.25 | 1.21 | 1.42 | 1.24 |
| d statistics (Durbin-Watson) | 1.13 | 1.30 | 1.24 | 1.19 | 1.19 | 1.19 | 1.10 | 1.07 | 1.40 | 1.25 | 1.55 | 1.62 | 1.41 | 1.65 |
| results of quantitative phase analyses [wt.%/100] | | | | | | | | | | | | | | |
| 1M phlogopite | 0.69 | 0.65 | 0.57 | 0.67 | 0.83 | 0.69 | 0.47 | 0.42 | 0.62 | 0.62 | 0.77 | 0.65 | 0.57 | 0.58 |
| $2M_1$ phlogopite | 0.21 | 0.25 | 0.32 | 0.19 | 0.17 | 0.22 | 0.33 | 0.34 | 0.31 | 0.28 | 0.18 | 0.21 | 0.26 | 0.18 |
| $2M_2$ phlogopite | 0.09 | 0.10 | 0.11 | 0.13 | - | 0.09 | 0.20 | 0.24 | 0.07 | 0.10 | 0.05 | 0.08 | 0.07 | 0.05 |
| quartz | - | - | - | 0.01 | - | - | - | - | - | - | - | - | - | - |
| sanidine | 0.01 | - | - | - | - | - | - | - | - | - | - | 0.06 | 0.10 | 0.19 |

Table 1. (cont.)

| run No. | SM 56-98 | SM 61-98 | SM 63-98 | SM 19-99 | SM 20-99 | SM 21-99 | SM 47-99 | SM 5-98 | SM 3-99 | SM 4-99 | SM 83-99 | SM 84-99 | SM 86-99 |
|---|---|---|---|---|---|---|---|---|---|---|---|---|---|
| temperature [°C] | 800 | 800 | 800 | 800 | 800 | 800 | 800 | 800 | 800 | 800 | 800 | 800 | 800 |
| pressure [MPa] | 200 | 2000 | 2000 | 200 | 200 | 200 | 200 | 200 | 200 | 200 | 2000 | 2000 | 200 |
| $X_K$(mica, see Table 2) | 0.00 | 0.80 | 0.59 | 0.80 | 0.79 | 0.69 | 0.82 | 0.01 | 0.70 | 0.83 | 0.73 | 0.80 | 0.74 |
| experimental series | **(K-Cs)-phlogopite series** | | | | | | | **(K-Ba)-phlogopite series** | | | | | |
| refinement details | | | | | | | | | | | | | |
| integrat.time/step interval [s] | 1080 | 793 | 793 | 792 | 660 | 540 | 300 | 650 | 528 | 427 | 488 | 427 | 600 |
| max. counts/step | 2435 | 2908 | 2906 | 3212 | 3238 | 2644 | 3376 | 3360 | 2945 | 2966 | 2747 | 3081 | 2820 |
| unique reflections | 2600 | 2458 | 2390 | 1480 | 3182 | 1492 | 1482 | 2471 | 2445 | 2435 | 5407 | 2439 | 3953 |
| structural parameters | 75 | 52 | 38 | 28 | 29 | 34 | 49 | 48 | 48 | 76 | 57 | 32 | 56 |
| experimental parameters | 37 | 26 | 21 | 23 | 26 | 23 | 23 | 30 | 24 | 24 | 25 | 23 | 26 |
| *N-P* | 5369 | 5870 | 5889 | 5897 | 5893 | 5881 | 5212 | 5870 | 5876 | 5848 | 5866 | 5893 | 5866 |
| *R* | 0.048 | 0.055 | 0.060 | 0.052 | 0.055 | 0.051 | 0.079 | 0.064 | 0.065 | 0.070 | 0.061 | 0.063 | 0.062 |
| $R_{wp}$ | 0.063 | 0.073 | 0.081 | 0.070 | 0.073 | 0.069 | 0.104 | 0.084 | 0.087 | 0.092 | 0.083 | 0.087 | 0.084 |
| $\chi 2$ | 1.90 | 1.25 | 1.56 | 1.24 | 1.32 | 1.21 | 1.50 | 1.92 | 1.38 | 1.62 | 1.46 | 1.44 | 1.55 |
| d statistics (Durbin-Watson) | 1.01 | 1.59 | 1.26 | 1.62 | 1.48 | 1.59 | 1.41 | 1.02 | 1.45 | 1.18 | 1.37 | 1.33 | 1.32 |
| results of quantitative phase analyses [wt.%/100] | | | | | | | | | | | | | |
| 1M phlogopite | 0.50 | 0.82 | 0.67 | 0.83 | 0.87 | 0.78 | 0.88 | 0.29 | 0.82 | 0.56 | 0.55 | 0.75 | 0.78 |
| $2M_1$ phlogopite | 0.27 | 0.14 | 0.31 | 0.17 | 0.07 | 0.22 | 0.12 | 0.54 | 0.17 | 0.34 | 0.34 | 0.21 | 0.12 |
| $2M_2$ phlogopite | 0.23 | 0.04 | - | - | 0.02 | - | - | 0.17 | 0.01 | 0.10 | 0.02 | 0.04 | 0.01 |
| quartz | - | - | - | - | 0.04 | - | - | - | - | - | - | - | - |
| celsian | - | - | - | - | - | - | - | - | - | - | - | - | 0.09 |
| cymrite | - | - | - | - | - | - | - | - | - | - | 0.09 | - | - |
| talc | - | - | 0.02 | - | - | - | - | - | - | - | - | - | - |

Bruker IFS 66v FTIR spectrometer equipped with a globar light source, a KBr-beam splitter and a DTGS-detector. Spectra were averaged over 256 scans. After linear background correction, the absorption band center, FWHM, and integral intensities were determined using the program *PeakFit* by JANDEL SCIENTIFIC.

## Results

### Optical investigations

The synthetic phlogopitic micas of the three experimental series generally occur as hexagonal platelets with diameters

Table 2. Results of EMP analyses of synthesized phlogopitic micas.

| run No. | SM 7-98 | SM 9-98 | SM 10-98 | SM 11-98 | SM 12-98 | SM 35-98 | SM 36-98 | SM 37-98 | SM 45-98 | SM 46-98 | SM 65-98 | SM 27-99 | SM 30-99 | SM 38-99 |
|---|---|---|---|---|---|---|---|---|---|---|---|---|---|---|
| analyses | 13 | 5 | 2 | 3 | 9 | 9 | 8 | 5 | 5 | 17 | 7 | 2 | 7 | 2 |
| exp. series | **(K-Rb)-phlogopite** | | | | | | | | | | | | | |
| wt.% of oxides | | | | | | | | | | | | | | |
| $SiO_2$ | 42.25 | 45.92 | 42.33 | 43.60 | 46.33 | 42.89 | 42.56 | 39.01 | 42.28 | 40.63 | 44.32 | 44.97 | 45.01 | 39.87 |
| $Al_2O_3$ | 9.80 | 10.97 | 11.35 | 9.90 | 10.24 | 12.37 | 12.05 | 10.36 | 11.22 | 11.64 | 10.56 | 10.72 | 9.78 | 10.22 |
| MgO | 24.61 | 27.59 | 25.52 | 25.17 | 27.45 | 28.08 | 27.82 | 23.53 | 27.03 | 26.92 | 27.19 | 27.57 | 27.73 | 24.94 |
| BaO | 0.00 | 0.00 | 0.00 | 0.00 | 0.00 | 0.00 | 0.00 | 0.00 | 0.00 | 0.00 | 0.00 | 0.00 | 0.00 | 0.00 |
| $K_2O$ | 3.23 | 7.91 | 7.69 | 3.81 | 8.07 | 7.19 | 5.63 | 0.02 | 3.51 | 2.55 | 5.22 | 7.87 | 7.17 | 2.53 |
| $Rb_2O$ | 12.20 | 1.14 | 2.55 | 9.38 | 0.20 | 4.36 | 8.19 | 20.48 | 12.70 | 15.04 | 6.59 | 0.02 | 3.09 | 13.27 |
| $Cs_2O$ | 0.00 | 0.00 | 0.00 | 0.00 | 0.00 | 0.00 | 0.00 | 0.00 | 0.00 | 0.00 | 0.00 | 0.00 | 0.00 | 0.00 |
| total | 92.09 | 93.53 | 89.44 | 91.85 | 92.29 | 94.89 | 96.25 | 93.40 | 96.74 | 96.77 | 93.87 | 91.15 | 92.77 | 90.82 |
| phlogopite composition on the basis of 22 oxygens | | | | | | | | | | | | | | |
| Si on IV | 6.43 | 6.40 | 6.27 | 6.50 | 6.50 | 6.07 | 6.07 | 6.22 | 6.16 | 6.02 | 6.36 | 6.38 | 6.42 | 6.23 |
| Al on IV | 1.57 | 1.60 | 1.73 | 1.50 | 1.50 | 1.93 | 1.93 | 1.78 | 1.84 | 1.98 | 1.64 | 1.62 | 1.58 | 1.77 |
| total IV | 8.00 | 8.00 | 8.00 | 8.00 | 8.00 | 8.00 | 8.00 | 8.00 | 8.00 | 8.00 | 8.00 | 8.00 | 8.00 | 8.00 |
| Al on VI | 0.19 | 0.21 | 0.25 | 0.23 | 0.19 | 0.13 | 0.10 | 0.17 | 0.09 | 0.06 | 0.15 | 0.18 | 0.07 | 0.11 |
| Mg on VI | 5.59 | 5.73 | 5.64 | 5.59 | 5.74 | 5.92 | 5.92 | 5.59 | 5.87 | 5.95 | 5.82 | 5.83 | 5.90 | 5.81 |
| total VI | 5.79 | 5.94 | 5.89 | 5.82 | 5.93 | 6.05 | 6.02 | 5.76 | 5.96 | 6.00 | 5.96 | 6.01 | 5.96 | 5.91 |
| K on XII | 0.63 | 1.41 | 1.45 | 0.72 | 1.44 | 1.30 | 1.03 | 0.00 | 0.65 | 0.48 | 0.96 | 1.42 | 1.30 | 0.50 |
| Rb on XII | 1.19 | 0.10 | 0.24 | 0.90 | 0.02 | 0.40 | 0.75 | 2.10 | 1.19 | 1.43 | 0.61 | 0.00 | 0.28 | 1.33 |
| Cs on XII | 0.00 | 0.00 | 0.00 | 0.00 | 0.00 | 0.00 | 0.00 | 0.00 | 0.00 | 0.00 | 0.00 | 0.00 | 0.00 | 0.00 |
| Ba on XII | 0.00 | 0.00 | 0.00 | 0.00 | 0.00 | 0.00 | 0.00 | 0.00 | 0.00 | 0.00 | 0.00 | 0.00 | 0.00 | 0.00 |
| total XII | 1.82 | 1.51 | 1.70 | 1.62 | 1.46 | 1.69 | 1.78 | 2.10 | 1.84 | 1.92 | 1.56 | 1.43 | 1.59 | 1.84 |
| occupancy of XII-sites (number of cations (p.f.u)/2), errors are 1σ-standard deviation of EMP analyses | | | | | | | | | | | | | | |
| $X_K$ | 0.31 | 0.70 | 0.73 | 0.36 | 0.72 | 0.65 | 0.51 | 0.00 | 0.33 | 0.24 | 0.48 | 0.71 | 0.65 | 0.25 |
| $\Delta X_K$ | 0.03 | 0.06 | 0.08 | 0.04 | 0.11 | 0.04 | 0.04 | 0.00 | 0.02 | 0.02 | 0.03 | 0.09 | 0.06 | 0.01 |
| $X_{Rb}$ | 0.60 | 0.05 | 0.12 | 0.45 | 0.01 | 0.20 | 0.38 | 1.05 | 0.59 | 0.72 | 0.30 | 0.00 | 0.14 | 0.67 |
| $\Delta X_{Rb}$ | 0.07 | 0.01 | 0.00 | 0.05 | 0.00 | 0.01 | 0.01 | 0.03 | 0.03 | 0.02 | 0.09 | 0.00 | 0.02 | 0.00 |
| $X_{Cs}$ | 0.00 | 0.00 | 0.00 | 0.00 | 0.00 | 0.00 | 0.00 | 0.00 | 0.00 | 0.00 | 0.00 | 0.00 | 0.00 | 0.00 |
| $\Delta X_{Cs}$ | 0.00 | 0.00 | 0.00 | 0.00 | 0.00 | 0.00 | 0.00 | 0.00 | 0.00 | 0.00 | 0.00 | 0.00 | 0.00 | 0.00 |
| $X_{Ba}$ | 0.00 | 0.00 | 0.00 | 0.00 | 0.00 | 0.00 | 0.00 | 0.00 | 0.00 | 0.00 | 0.00 | 0.00 | 0.00 | 0.00 |
| $\Delta X_{Ba}$ | 0.00 | 0.00 | 0.00 | 0.00 | 0.00 | 0.00 | 0.00 | 0.00 | 0.00 | 0.00 | 0.00 | 0.00 | 0.00 | 0.00 |
| $X_{\square}$ | 0.09 | 0.25 | 0.15 | 0.19 | 0.27 | 0.15 | 0.11 | 0.00 | 0.08 | 0.04 | 0.22 | 0.29 | 0.21 | 0.08 |
| $\Delta X_{\square}$ | 0.03 | 0.03 | 0.04 | 0.03 | 0.06 | 0.02 | 0.02 | 0.02 | 0.02 | 0.02 | 0.05 | 0.05 | 0.03 | 0.00 |

up to 30 μm (*cf.*, Fig. 1 in Melzer & Wunder, 2001). The thickness of the platelets ranges between 1 and 5 μm.

## XRD investigations

Quantitative determination of phase proportions were performed by Rietveld analyses of XRD diffractograms. The results are compiled in Table 1 and showed that all runs yielded between 81 and 100 wt.% of phlogopitic micas. Quartz and sanidine were determined in some of the experiments from the (K-Rb)- and (K-Cs)-series. Talc as additional phase was observed in run SM63-98 of the (K-Cs)-series. The Ba-bearing phases celsian and cymrite appeared as additional phases in the runs SM83-99 and SM86-99 of the (K-Ba)-series.

The most abundant polytype in all runs is the one-layer monoclinic polytype (1*M*) except of run SM5-98, where the principle polytype is the two-layer polytype $2M_1$. Besides these two polytypes, which were detected in all runs, the two-layer polytype $2M_2$ was found in small amounts within several run products. No other polytypes were detected (Table 1).

## EMP analyses

Table 2 shows the mean values of all accepted phlogopite EMP analyses and calculated site occupancies. Formulae of phlogopitic mica were calculated on the basis of 22 oxygens per formula unit. The cation occupancies were determined in such a way that the T-sites are completely filled with $Si^{4+}$ and $Al^{3+}$, the M-sites with the $Mg^{2+}$ cations plus the remaining $Al^{3+}$, and the interlayers with the monovalent alkalis $K^+$, $Rb^+$ and $Cs^+$ and, for the third series the divalent $Ba^{2+}$.

Fig. 1a–c show the interlayer occupancies of the synthesized phlogopitic micas. Mean values for each run are taken from Table 2. As intended by the experimental approach, the produced phlogopitic micas are mainly solid solutions between phlogopite and Rb-phlogopite (Fig. 1a), phlogopite and Cs-phlogopite (Fig. 1b) and phlogopite and kinoshitali-

Table 2. (cont.)

| run No. | SM 56-98 | SM 61-98 | SM 63-98 | SM 19-99 | SM 20-99 | SM 21-99 | SM 47-99 | SM 5-98 | SM 3-99 | SM 4-99 | SM 83-99 | SM 84-99 | SM 86-99 |
|---|---|---|---|---|---|---|---|---|---|---|---|---|---|
| analyses | 2 | 10 | 5 | 3 | 5 | 6 | 3 | 3 | 6 | 9 | 7 | 8 | 6 |
| exp. series | | | | **(K-Cs)-phlogopite** | | | | | | **(K-Ba)-phlogopite** | | | |
| wt.% of oxides | | | | | | | | | | | | | |
| $SiO_2$ | 34.16 | 44.30 | 43.67 | 43.29 | 41.91 | 40.84 | 41.23 | 24.11 | 43.64 | 45.20 | 44.35 | 44.75 | 42.64 |
| $Al_2O_3$ | 9.59 | 12.02 | 12.72 | 11.25 | 10.99 | 14.70 | 12.51 | 18.45 | 13.02 | 11.74 | 12.85 | 13.48 | 10.59 |
| MgO | 20.11 | 28.30 | 26.79 | 26.52 | 25.55 | 26.41 | 26.24 | 22.52 | 25.91 | 26.20 | 26.26 | 25.44 | 25.32 |
| BaO | 0.00 | 0.00 | 0.00 | 0.00 | 0.00 | 0.00 | 0.00 | 26.94 | 1.32 | 0.53 | 2.33 | 0.99 | 2.86 |
| $K_2O$ | 0.01 | 8.96 | 6.56 | 8.61 | 8.24 | 7.45 | 8.77 | 0.11 | 7.74 | 9.22 | 8.11 | 9.01 | 7.79 |
| $Rb_2O$ | 0.00 | 0.00 | 0.00 | 0.00 | 0.00 | 0.00 | 0.00 | 0.00 | 0.00 | 0.00 | 0.00 | 0.00 | 0.00 |
| $Cs_2O$ | 26.86 | 1.30 | 5.17 | 1.81 | 2.82 | 4.03 | 1.67 | 0.00 | 0.00 | 0.00 | 0.00 | 0.00 | 0.00 |
| total | 90.73 | 94.88 | 94.92 | 91.48 | 89.50 | 93.44 | 90.43 | 92.13 | 91.64 | 92.90 | 93.89 | 93.67 | 89.21 |
| phlogopite composition on the basis of 22 oxygens | | | | | | | | | | | | | |
| Si on IV | 6.21 | 6.17 | 6.20 | 6.27 | 6.26 | 5.89 | 6.06 | 4.24 | 6.22 | 6.36 | 6.23 | 6.26 | 6.35 |
| Al on IV | 1.79 | 1.83 | 1.80 | 1.73 | 1.74 | 2.11 | 1.94 | 3.76 | 1.78 | 1.64 | 1.77 | 1.74 | 1.65 |
| total IV | 8.00 | 8.00 | 8.00 | 8.00 | 8.00 | 8.00 | 8.00 | 8.00 | 8.00 | 8.00 | 8.00 | 8.00 | 8.00 |
| Al on VI | 0.27 | 0.14 | 0.32 | 0.19 | 0.20 | 0.38 | 0.23 | 0.07 | 0.41 | 0.31 | 0.36 | 0.48 | 0.20 |
| Mg on VI | 5.45 | 5.87 | 5.67 | 5.73 | 5.69 | 5.67 | 5.75 | 5.91 | 5.50 | 5.50 | 5.50 | 5.30 | 5.62 |
| total VI | 5.72 | 6.01 | 5.99 | 5.92 | 5.89 | 6.06 | 5.98 | 5.98 | 5.91 | 5.81 | 5.85 | 5.78 | 5.82 |
| K on XII | 0.00 | 1.59 | 1.19 | 1.59 | 1.57 | 1.37 | 1.65 | 0.02 | 1.41 | 1.65 | 1.45 | 1.61 | 1.48 |
| Rb on XII | 0.00 | 0.00 | 0.00 | 0.00 | 0.00 | 0.00 | 0.00 | 0.00 | 0.00 | 0.00 | 0.00 | 0.00 | 0.00 |
| Cs on XII | 2.08 | 0.08 | 0.31 | 0.11 | 0.18 | 0.25 | 0.10 | 0.00 | 0.00 | 0.00 | 0.00 | 0.00 | 0.00 |
| Ba on XII | 0.00 | 0.00 | 0.00 | 0.00 | 0.00 | 0.00 | 0.00 | 1.86 | 0.07 | 0.03 | 0.13 | 0.05 | 0.17 |
| total XII | 2.09 | 1.67 | 1.50 | 1.70 | 1.75 | 1.62 | 1.75 | 1.88 | 1.48 | 1.68 | 1.58 | 1.66 | 1.65 |
| occupancy of XII-sites (number of cations (p.f.u)/2), errors are 1σ-standard deviation of EMP analyses | | | | | | | | | | | | | |
| $X_K$ | 0.00 | 0.80 | 0.59 | 0.80 | 0.79 | 0.69 | 0.82 | 0.01 | 0.70 | 0.83 | 0.73 | 0.80 | 0.74 |
| $\Delta X_K$ | 0.00 | 0.05 | 0.03 | 0.06 | 0.06 | 0.10 | 0.05 | 0.00 | 0.13 | 0.08 | 0.03 | 0.02 | 0.05 |
| $X_{Rb}$ | 0.00 | 0.00 | 0.00 | 0.00 | 0.00 | 0.00 | 0.00 | 0.00 | 0.00 | 0.00 | 0.00 | 0.00 | 0.00 |
| $\Delta X_{Rb}$ | 0.00 | 0.00 | 0.00 | 0.00 | 0.00 | 0.00 | 0.00 | 0.00 | 0.00 | 0.00 | 0.00 | 0.00 | 0.00 |
| $X_{Cs}$ | 1.04 | 0.04 | 0.16 | 0.06 | 0.09 | 0.12 | 0.05 | 0.00 | 0.00 | 0.00 | 0.00 | 0.00 | 0.00 |
| $\Delta X_{Cs}$ | 0.02 | 0.00 | 0.03 | 0.00 | 0.02 | 0.01 | 0.00 | 0.00 | 0.00 | 0.00 | 0.00 | 0.00 | 0.00 |
| $X_{Ba}$ | 0.00 | 0.00 | 0.00 | 0.00 | 0.00 | 0.00 | 0.00 | 0.93 | 0.04 | 0.01 | 0.06 | 0.03 | 0.08 |
| $\Delta X_{Ba}$ | 0.00 | 0.00 | 0.00 | 0.00 | 0.00 | 0.00 | 0.00 | 0.08 | 0.00 | 0.01 | 0.01 | 0.01 | 0.02 |
| $X_{\square}$ | -0.04 | 0.17 | 0.25 | 0.15 | 0.12 | 0.19 | 0.12 | 0.06 | 0.26 | 0.16 | 0.21 | 0.17 | 0.18 |
| $\Delta X_{\square}$ | 0.01 | 0.03 | 0.02 | 0.03 | 0.03 | 0.05 | 0.02 | 0.04 | 0.06 | 0.04 | 0.02 | 0.01 | 0.03 |

te (Fig. 1c). For both, the (K-Cs)- and the (K-Ba)-series, besides Cs-phlogopite and kinoshitalite, only phlogopites close to the K-endmember have been synthesized. This does not indicate a miscibility gap and only results from the compositions of the starting bulks, which were mostly chosen to lie close to the K-endmember. Almost all phlogopites show significant concentrations of interlayer vacancies up to a maximum value of 29 mole % (Table 2, Fig. 1a–c). A positive correlation between the interlayer vacancy concentration and the Rb-content (Fig. 1a) is obvious for the (K-Rb)-series. Interlayer vacancies require a charge compensation, either by the substitution of $Al^{3+}$ by $Si^{4+}$ at the tetrahedral sites or $Mg^{2+}$ by $Al^{3+}$ at the octahedral sites. In Fig. 2, the average molar fractions of Si, Mg and Al for phlogopites from each experiment are shown. All compositions, except for the Ba-endmember kinoshitalite (run SM5-98), lie within the triangle talc – phlogopite – eastonite ($KMg_{2.5}Al_{0.5}[Si_{2.5}Al_{1.5}O_{10}](OH)_2$), shown in detail in Fig. 3. Phlogopites, for which the composition is located below the join phlogopite – celadonite ($KAlMg[Si_4O_{10}](OH)_2$) are solid solutions of phlogopite, eastonite and celadonite. Starting from phlogopite, variations on T- and M-sites may therefore be explained by the two exchange vectors $^{VI}Mg_{-1}{}^{IV}Si_{-1}{}^{VI}Al_1{}^{IV}Al_1$ and $^{VI}Mg_{-2}{}^{IV}Al_{-1}{}^{IV}Si_1{}^{VI}Al_1{}^{VI}\square_1$. However, all phlogopitic micas with compositions above the join phlogopite – celadonite (grey area of Fig. 3) must have a talc component. According to the exchange vector $^{XII}K_{-1}{}^{IV}Al_{-1}{}^{XII}\square_1{}^{IV}Si_1$ this talc component within phlogopite is combined with the formation of interlayer vacancies.

## IR spectroscopy

The variations of IR spectra in the spectral range 3550 to 3800 $cm^{-1}$ for the (K-Rb)-series are presented in Fig. 4a. All IR spectra of the (K-Rb)-series exhibit a strong OH-band, labelled the N-band after Vedder (1964), with a band maximum at about 3720 $cm^{-1}$ and a FWHM of about 13 $cm^{-1}$. Compared to pure phlogopite (3724 $cm^{-1}$) the N-band of the synthetic phlogopitic micas is generally shifted to lower en-

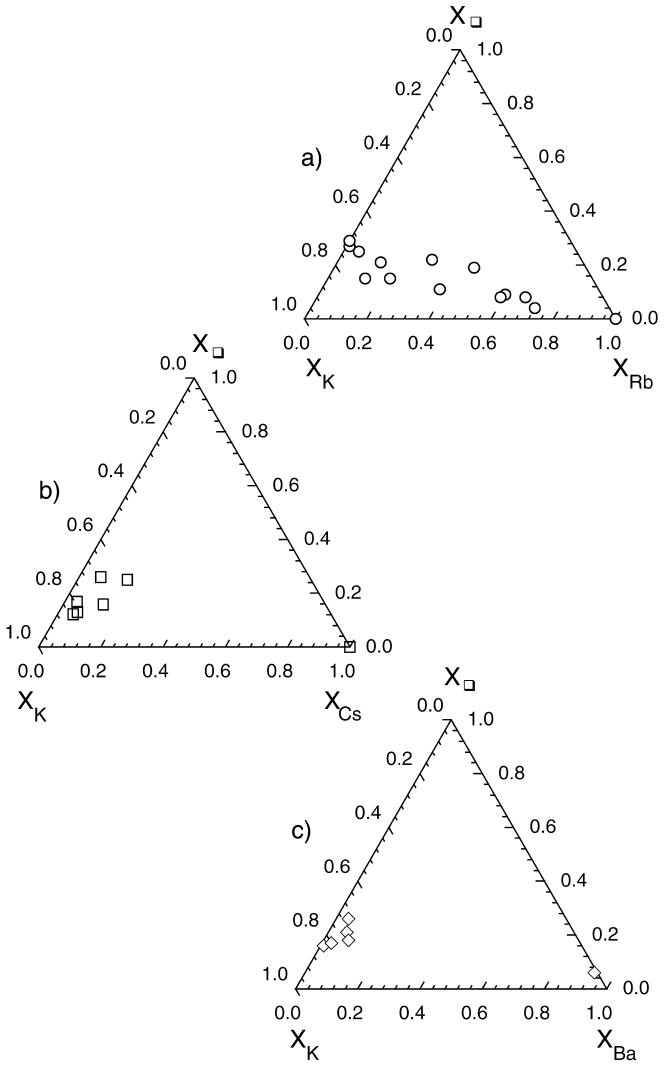


Fig. 1. Occupancy of the interlayer sites in terms of molar fractions of K, Rb, Cs, Ba, and □ for the three experimental series as determined by EMP analyses.

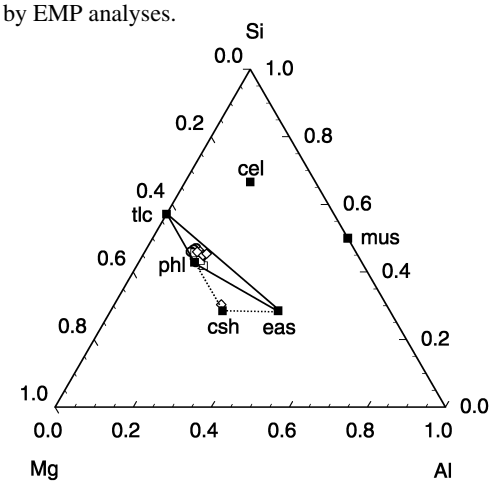


Fig. 2. Mean phlogopite compositions of each sample of the three experimental series in terms of molar fractions of Si, Al, and Mg at the tetrahedral and octahedral sites plotted in a ternary diagram Mg – Al – Si. Symbols: ○ (K-Rb-series), □ (K-Cs-series), ◇ (K-Ba-series). Abbreviations: phl: phlogopite, eas: eastonite, cel: celadonite, tlc: talc, mus: muscovite, csh: kinoshitalite.

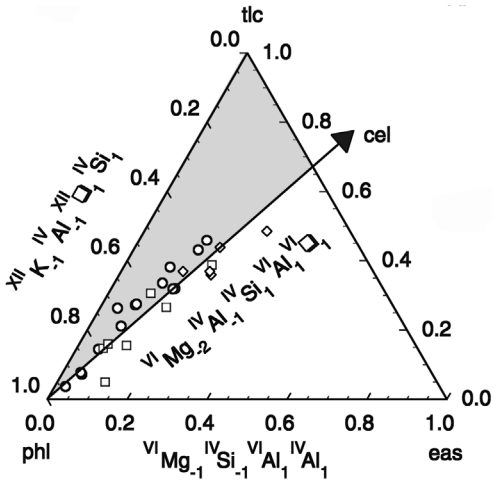


Fig. 3. Phlogopite compositions of each sample of the three experimental series plotted within the ternary system phlogopite – eastonite – talc. Symbols: ○ (K-Rb-series), □ (K-Cs-series), ◇ (K-Ba-series). Abbreviations: phl: phlogopite, eas: eastonite, cel: celadonite, tlc: talc.

ergies. A distinct shoulder on the low-energy side is visible for the samples SM37-98 and SM7-98. A strong asymmetry towards lower wavenumbers of the N-band appears in all other spectra. For fitting the band system of the N-band range, we assume up to three distinct OH-bands (Table 3). Both, the decrease of N-band wavenumbers and the existence of a fine structure of OH-stretching bands of phlogopitic micas was explained by Robert & Kodama (1988) as the result of a modification of the charge distribution around the OH-group by incorporation of Al in tetrahedral and octahedral layers. However, our EMP and IR data indicate that the shift of the N-band towards lower energies is also correlated with increasing Rb-content. For pure Rb-phlogopite (SM37-98) the N-band is located at 3718 $cm^{-1}$. OH-stretching bands with very low intensities but larger FWHM were observed in some of the spectra: the V-bands ($Al^{3+}Al^{3+}\square^{VI}$) at around 3600 $cm^{-1}$ (*cf.,* run SM30-99) and the I-bands ($Mg^{2+}Mg^{2+}Al^{3+}$) at about 3650 $cm^{-1}$ (*cf.*, run SM27-99). An additional band appears in the energy-range 3674 – 3678 $cm^{-1}$, here termed $V^{*}$-band. Comparing the results of the EMP analyses (Table 2) with the integral intensity of the $V^{*}$-band, it is clear that this intensity is inversely correlated with the interlayer occupancy (Fig 4a). The $V^{*}$-band is therefore interpreted as representing the talc component within the phlogopitic mica and not by chemical variations at M- and T-sites within the mica structure.

For the (K-Cs)-series, the N-band at about 3720 $cm^{-1}$ exhibits the highest intensity (Fig. 4b). In analogy to the (K-Rb)-series, the maximum of this band is shifted towards lower energies for increasing Cs-contents and is located at 3711 $cm^{-1}$ for pure Cs-phlogopite (SM56-98). The FWHM of the N-band ranges between 11 and 15 $cm^{-1}$ and does not show any systematic variation with increasing Cs-concentration. Broad low-intensity I- and V-bands are present in some of the spectra from the (K-Cs)-series. The $V^{*}$-band at about 3676 $cm^{-1}$ is also present, and, in analogy to the (K-

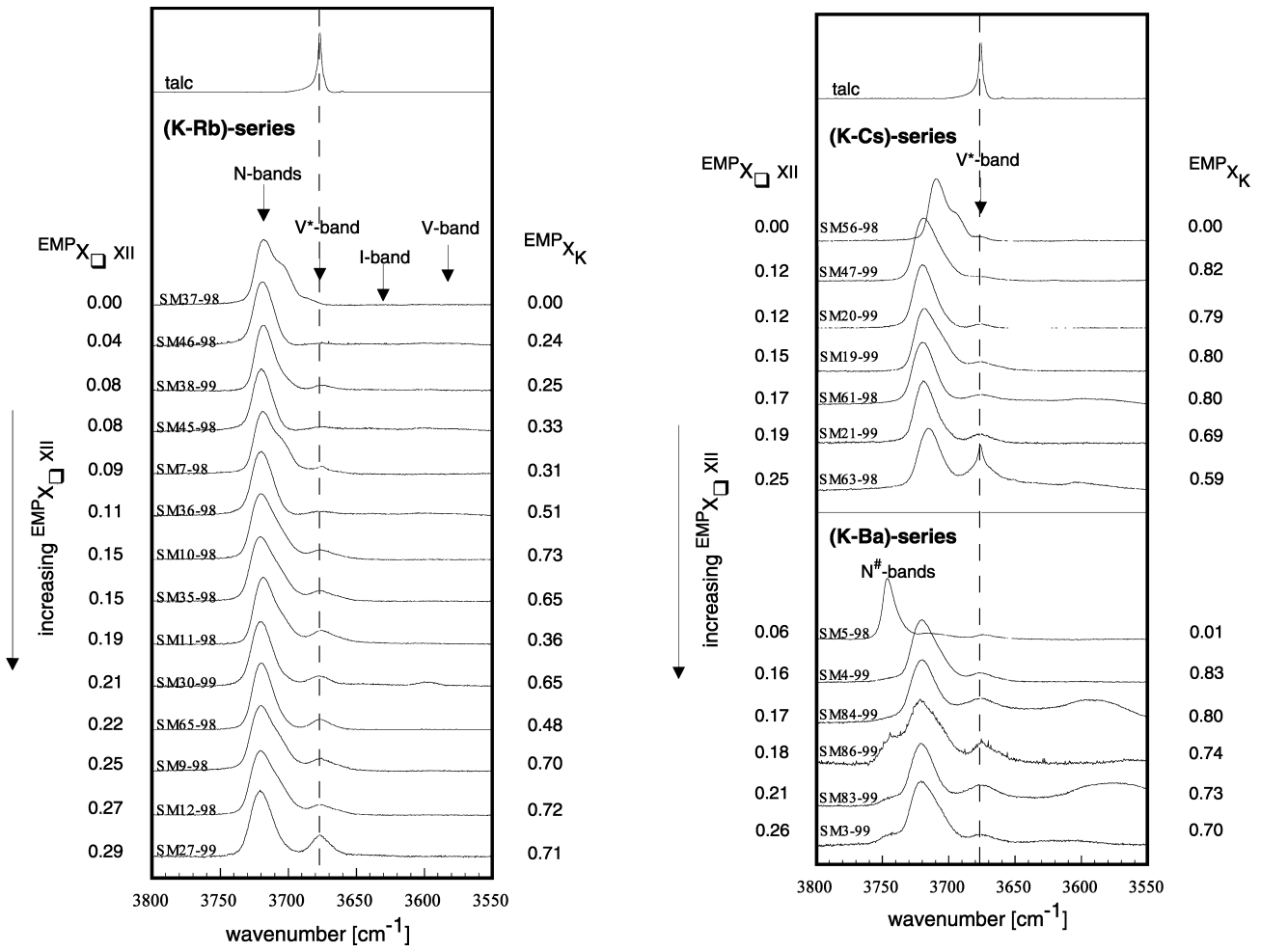


Fig. 4a–c. IR spectra of run products of the (K-Rb)-series (a), (K-Cs)-series (b), and (K-Ba)-series (c) in the spectral region of the OH-stretching vibration. See text for explanations of the various OH-bands.

Rb)-series, its integral intensity is correlated with the amount of the EMP-determined interlayer vacancy concentrations (Table 2, Fig. 4b). For the V*-band, the FWHM lies between 12 $cm^{-1}$ and 36 $cm^{-1}$.

Fig. 4c shows the IR spectra determined for the (K-Ba)-series. For phlogopitic mica with moderate Ba-contents ($X_{Ba}$ < 0.1) the band with the highest intensity is located at about 3723 $cm^{-1}$ and is classified as the N-band. In contrast to the (K-Rb)- and (K-Cs)-series, an additional band, labelled N#-band here, appears on the high energy side of the N-band at 3743 $cm^{-1}$. The intensity of the additional N#-band continuously increases with increasing Ba-concentration, whereas the intensity of the N-band continuously decreases. Consequently, for nearly pure kinoshitalite (SM5-98) the N-band at 3716 $cm^{-1}$ mostly disappeared and the main N#-band lies at 3747 $cm^{-1}$ (Fig. 4c). The FWHM of both, the N- and N#-band are comparable and range between 8 and 36 $cm^{-1}$. For brittle mica endmember kinoshitalite, the local cation coordination around the hydroxyl that produces the N#-band can be ascribed to $Ba^{XII}(MgMgMg)^{VI}Al^{IV}$. Such a high-energy frequency band (3735 $cm^{-1}$) is also known from Ba-containing vermiculites (Fernandez *et al.*, 1970), and was explained by Farmer (1974) as a shift of the ($Mg_3OH$)-frequency due to the higher electronegativity of $Ba^{2+}$ (1.0) in comparison to $Rb^+$ and $Cs^+$ (0.9), which would force the hydroxyl group away from the perpendicular orientation. The N#-band, observed for the nearly alkali-free run SM5-98, shows a strong asymmetry to lower wavenumbers, which could only be fitted by assuming two further destinct bands (Table 3). Only for the runs SM83-99 and SM84-99 V-bands located at around 3575 $cm^{-1}$ and 3590 $cm^{-1}$ are detectable. Beside these OH-bands, only the V*-band at about 3676 $cm^{-1}$ is present in all products. In analogy to the (K-Rb)- and (K-Cs)-series, a distinct correlation between the intensity of this band and the amount of $\square^{XII}$ as determined by EMP (Table 2, Fig. 4c) is obvious.

## Discussion

A significant correlation between the interlayer vacancy concentrations determined by EMP (Table 2) and the intensity of the V*-band observed in the range 3674 – 3678 $cm^{-1}$ is obvious (Fig. 4a–c). The V*-band corresponds to the main OH-frequency of talc lying at 3677 $cm^{-1}$ after Vedder (1964), which is, for comparison, shown in Fig. 4a,b. As dis-

Table 3. Results of IR spectroscopic measurements and derived vacancy concentrations on the interlayer site.

| run No. | | SM 7-98 | SM 9-98 | SM 10-98 | SM 11-98 | SM 12-98 | SM 35-98 | SM 36-98 | SM 37-98 | SM 45-98 | SM 46-98 | SM 65-98 | SM 27-99 | SM 30-99 | SM 38-99 |
|---|---|---|---|---|---|---|---|---|---|---|---|---|---|---|---|
| experimental series | | **(K-Rb)-phlogopite** | | | | | | | | | | | | | |
| N-bands | | | | | | | | | | | | | | | |
| location | $N_1$ | 3702 | 3703 | 3702 | 3701 | 3703 | 3708 | 3711 | 3700 | 3711 | 3711 | | 3705 | 3702 | 3701 |
| | $N_3$ | 3710 | 3712 | 3712 | 3711 | 3713 | 3715 | 3717 | 3708 | 3716 | 3717 | 3710 | 3716 | 3714 | 3711 |
| | $N_3$ | 3719 | 3722 | 3722 | 3720 | 3723 | 3723 | 3723 | 3718 | 3723 | 3722 | 3720 | 3723 | 3723 | 3720 |
| integral absorbance $A_N$ | $N_1$ | 0.45 | 0.42 | 0.39 | 0.30 | 0.39 | 0.24 | 0.34 | 0.52 | 0.19 | 0.40 | | 0.15 | 0.10 | 0.13 |
| | $N_2$ | 0.53 | 0.68 | 0.82 | 0.54 | 0.73 | 0.91 | 0.87 | 0.55 | 0.79 | 0.69 | 0.42 | 0.59 | 0.52 | 0.39 |
| | $N_3$ | 1.21 | 1.30 | 1.50 | 1.10 | 1.31 | 1.31 | 1.16 | 1.37 | 1.06 | 0.92 | 1.43 | 0.91 | 1.08 | 0.91 |
| | $\Sigma N_i$ | 2.18 | 2.41 | 2.70 | 1.95 | 2.43 | 2.46 | 2.37 | 2.44 | 2.04 | 2.02 | 1.85 | 1.64 | 1.70 | 1.44 |
| FWHM | $N_{1-3}$ | 13 | 14 | 14 | 13 | 14 | 14 | 12 | 13 | 12 | 11 | 14 | 14 | 14 | 12 |
| V*-band | | | | | | | | | | | | | | | |
| location | | 3678 | 3676 | 3676 | 3676 | 3676 | 3676 | 3674 | | 3675 | 3675 | 3676 | 3676 | 3678 | 3676 |
| integral absorbance $A_{V*}$ | | 0.20 | 0.41 | 0.36 | 0.37 | 0.41 | 0.45 | 0.11 | | 0.09 | 0.05 | 0.30 | 0.59 | 0.23 | 0.10 |
| FWHM | | 29 | 25 | 23 | 26 | 56 | 25 | 18 | | 16 | 15 | 17 | 17 | 17 | 17 |
| I-band | | | | | | | | | | | | | | | |
| location | | | | 3659 | 3656 | | 3646 | | | 3648 | 3646 | | 3641 | 3646 | 3648 |
| integral absorbance $A_I$ | | | | 0.02 | 0.24 | | 0.49 | | | 0.14 | 0.08 | | 0.02 | 0.11 | 0.11 |
| FWHM | | | | 14 | 45 | | 60 | | | 35 | 35 | | 26 | 44 | 67 |
| V-band | | | | | | | | | | | | | | | |
| location | | | | | | | 3594 | 3609 | | 3594 | 3592 | | | 3598 | 3599 |
| integral absorbance $A_V$ | | | | | | | 0.37 | 0.34 | | 0.23 | 0.19 | | | 0.09 | 0.03 |
| FWHM | | | | | | | 47 | 84 | | 50 | 50 | | | 18 | 26 |
| calculated vacancy concentrations on XII | | | | | | | | | | | | | | | |
| spec. integral absorbance | | 0.09 | 0.17 | 0.15 | 0.16 | 0.17 | 0.19 | 0.05 | 0.00 | 0.04 | 0.02 | 0.13 | 0.25 | 0.11 | 0.05 |
| $X_\square$ on XII (IR) | | 0.11 | 0.21 | 0.19 | 0.21 | 0.21 | 0.24 | 0.06 | 0.00 | 0.05 | 0.03 | 0.16 | 0.33 | 0.14 | 0.07 |
| $X_\square$ on XII (EMP) | | 0.09 | 0.25 | 0.15 | 0.19 | 0.27 | 0.15 | 0.11 | 0.00 | 0.08 | 0.04 | 0.22 | 0.29 | 0.21 | 0.08 |
| Deviation | | 0.11 | -0.03 | 0.04 | 0.02 | -0.05 | 0.09 | -0.05 | 0.00 | -0.03 | -0.02 | -0.05 | 0.04 | -0.07 | -0.01 |
| $\Delta X_\square$ on XII (IR) | | 0.04 | 0.04 | 0.04 | 0.04 | 0.04 | 0.04 | 0.04 | 0.05 | 0.04 | 0.04 | 0.04 | 0.05 | 0.05 | 0.05 |
| $\Delta X_\square$ on XII (EMP) | | 0.06 | 0.06 | 0.08 | 0.07 | 0.11 | 0.04 | 0.04 | 0.03 | 0.04 | 0.03 | 0.09 | 0.09 | 0.07 | 0.01 |

$\Delta X_\square$ on XII (EMP) are 2σ-standard deviation of the EMP analyses, $\Delta X_\square$ on XII (IR) correspond to a 10% relative error of the intensity of the V*-band.

‡ corrected for additional phases and normalized for the molar mass of phlogopite (see text)

cussed above, interlayer vacancies within phlogopitic micas require a charge compensation either by the substitution of (1) $Al^{3+}$ by $Si^{4+}$ at tetrahedral sites leading to a local talc configuration, or (2) $Mg^{2+}$ by $Al^{3+}$ at the octahedral sites. Indeed, according to Robert & Kodama (1988), OH-bands lying between 3650 and 3675 $cm^{-1}$ should be attributed to some Al on octahedral sites. If substitution (2) is relevant, a correlation of the intensity of the $V^*$-band and I-band should exist. This is, however, not the case (Table 3). Additionally, the amount of octahedral Al in the synthesized phlogopitic micas is extremely low (Table 2) and shows no correlation with the intensity of the $V^*$-band. We therefore assume that the $V^*$-band exhibits information about the vacancy concentration on the twelve-fold position representing the talc component of phlogopitic micas and that (1) ($Al^{3+}$ by $Si^{4+}$ at tetrahedral sites) is the relevant substitution mechanism. The local coordination around hydroxyl that produces the $V^*$-band is therefore $\square^{XII}(MgMgMg)^{VI}Si^{IV}$.

Based on these considerations, the integral intensity of the $V^*$-band $A_V$* was determined for both, synthetic phlogopitic micas of the three experimental series (Table 3) and synthetic talc of the endmember composition $Mg_3Si_4O_{10}(OH)_2$, previously synthesized as a single phase and characterized by Wunder *et al.* (1997). The weighted portion of the run products were corrected for additional phases and normalized to the molar mass of phlogopitic mica. This resulted in specific integral intensities (Table 3). The coefficient of the normalized band intensities of phlogopitic micas and talc represents the IR-determined interlayer vacancy concentration ($^{IR}X_\square^{XII}$) of phlogopitic micas. The dependence of the linear absorption coefficient as a function of the wavenumber (Libowitzky & Rossman, 1997) was not considered, because the structural similar materials talc and phlogopite absorb IR radiation in the same frequency range. The procedure resulting in the concentration of $^{IR}X_\square^{XII}$ is expressed by:

$$^{IR}X_\square^{XII} = \frac{A_V^*\,(3674 - 3678\ cm^{-1},\ mica)\ /\ [wt.\%(mica,\ Rietveld)/(M(mica)\cdot 1000)]}{A_V^*(3676\ cm^{-1},talc)/[1/M(talc)\cdot 10]} \quad (1)$$

The derived $^{IR}X_\square^{XII}$ concentations are listed in Table 3 and are plotted against the vacancy concentration ($^{EMP}X_\square^{XII}$) as determined by EMP in Fig. 5. Most of calculated vacancy concentrations $^{IR}X_\square^{XII}$ are, within the assumed uncertain-

Table 3. (cont.)

| run No. | | SM 56-98 | SM 61-98 | SM 63-98 | SM 19-99 | SM 20-99 | SM 21-99 | SM 47-99 | SM 5-98 | SM 3-99 | SM 4-99 | SM 83-99 | SM 84-99 | SM 86-99 |
|---|---|---|---|---|---|---|---|---|---|---|---|---|---|---|
| experimental series | | (K-Cs)-phlogopite | | | | | | | (K-Ba)-phlogopite | | | | | |
| N-bands | | | | | | | | | | | | | | |
| location | $N_1$ | 3694 | 3708 | 3703 | 3701 | | 3703 | 3702 | | 3702 | 3702 | 3700 | 3697 | 3702 |
| | $N_2$ | 3703 | 3716 | 3712 | 3711 | 3710 | 3713 | 3712 | | 3712 | 3712 | 3713 | 3711 | 3711 |
| | $N_3$ | 3711 | 3724 | 3719 | 3721 | 3721 | 3721 | 3722 | 3716 | 3723 | 3723 | 3723 | 3722 | 3724 |
| integral absorbance $A_N$ | $N_1$ | 0.45 | 0.26 | 0.19 | 0.32 | | 0.41 | 0.33 | | 0.26 | 0.26 | 0.07 | 0.12 | 0.12 |
| | $N_2$ | 0.53 | 0.91 | 0.63 | 0.65 | 0.46 | 1.28 | 0.76 | | 0.59 | 0.65 | 0.39 | 0.39 | 0.24 |
| | $N_3$ | 1.13 | 1.16 | 0.81 | 1.18 | 1.40 | 2.17 | 1.26 | 0.37 | 0.97 | 1.10 | 0.80 | 0.77 | 0.48 |
| | $\Sigma N_i$ | 2.11 | 2.32 | 1.62 | 2.15 | 1.87 | 3.86 | 2.35 | 0.37 | 1.82 | 2.01 | 1.26 | 1.29 | 0.84 |
| FWHM | $N_{1-3}$ | 11 | 13 | 14 | 14 | 15 | 13 | 13 | 36 | 15 | 14 | 16 | 17 | 17 |
| $N^{\#}$-bands | | | | | | | | | | | | | | |
| location | $N_1^{\#}$ $N_1$ | | | | | | | | 3734 | 3744 | 3742 | 3743 | 3742 | 3744 |
| | $N_2^{\#}$ | | | | | | | | 3741 | | | | | |
| | $N_3^{\#}$ | | | | | | | | 3747 | | | | | |
| integral absorbance $A_N$# | $N_1^{\#}$ | | | | | | | | 0.13 | 0.18 | 0.12 | 0.13 | 0.17 | 0.23 |
| | $N_2^{\#}$ | | | | | | | | 0.35 | | | | | |
| | $N_3^{\#}$ | | | | | | | | 1.00 | | | | | |
| | $\Sigma N_i^{\#}$ | | | | | | | | 1.48 | 0.18 | 0.12 | 0.12 | 0.17 | 0.23 |
| FWHM | $N_{1-3}^{\#}$ | | | | | | | | 8 | 16 | 14 | 16 | 22 | 16 |
| V*-band | | | | | | | | | | | | | | |
| location | | 3677 | 3677 | 3678 | 3678 | 3676 | 3675 | 3674 | 3673 | 3675 | 3677 | 3677 | 3678 | 3674 |
| integral absorbance $A_{V*}$ | | 0.07 | 0.30 | 0.57 | 0.47 | 0.05 | 0.43 | 0.25 | 0.20 | 0.45 | 0.37 | 0.49 | 0.43 | 0.38 |
| FWHM | | 13 | 24 | 25 | 31 | 12 | 19 | 36 | 19 | 28 | 25 | 28 | 27 | 25 |
| I-bands | | | | | | | | | | | | | | |
| location | | | 3650 | 3652 | | | | | | 3630 | | 3651 | 3652 | |
| integral absorbance $A_I$ | | | 0.44 | 0.34 | | | | | | 0.08 | | 0.51 | 0.64 | |
| FWHM | | | 76 | 42 | | | | | | 25 | | 83 | 57 | |
| V-bands | | | | | | | | | | | | | | |
| location | | | 3590 | 3600 | | | | | | 3604 | | 3575 | 3590 | 3561 |
| integral absorbance $A_V$ | | | 0.36 | 0.32 | | | | | | 0.18 | | 1.43 | 1.26 | 0.09 |
| FWHM | | | 46 | 45 | | | | | | 38 | | 64 | 57 | 42 |
| calculated vacancy concentrations on XII | | | | | | | | | | | | | | |
| spec. integral absorb. $A_{V*}^{+}_{+}$ | | 0.04 | 0.12 | 0.24 | 0.25 | 0.02 | 0.09 | 0.11 | 0.10 | 0.19 | 0.15 | 0.22 | 0.18 | 0.17 |
| $X_{\square}$ on XII (IR) | | 0.05 | 0.16 | 0.31 | 0.19 | 0.03 | 0.12 | 0.14 | 0.13 | 0.24 | 0.19 | 0.29 | 0.23 | 0.22 |
| $X_{\square}$ on XII (EMP) | | -0.04 | 0.17 | 0.25 | 0.15 | 0.12 | 0.19 | 0.12 | 0.06 | 0.26 | 0.16 | 0.21 | 0.17 | 0.18 |
| deviation | | 0.09 | -0.01 | 0.06 | 0.04 | -0.09 | -0.07 | 0.02 | 0.07 | 0.02 | 0.03 | 0.08 | 0.05 | 0.04 |
| $\Delta X_{\square}$ on XII (IR) | | 0.05 | 0.04 | 0.04 | 0.04 | 0.04 | 0.04 | 0.04 | 0.05 | 0.04 | 0.04 | 0.05 | 0.04 | 0.05 |
| $\Delta X_{\square}$ on XII (EMP) | | 0.02 | 0.05 | 0.04 | 0.06 | 0.06 | 0.10 | 0.05 | 0.08 | 0.13 | 0.08 | 0.03 | 0.02 | 0.06 |

$^{+}_{+}$ corrected for additional phases and normalized for the molar mass of phlogopite (see text)

ties, in agreement to the $^{EMP}X_{\square}^{XII}$ concentations. However, for a reliable spectroscopically quantification of interlayer vacancy concentrations, uncertainties are too high. The scattering shown in Fig. 5 has different reasons: *e.g.* it might be due to variations in the local structure of the micas, for which varying absorption coefficients have to be expected. Other problems might be the determination of the integrated intensities from the KBr-pellets, in which the platy crystals might be oriented during pressurization, or even inhomogeneity of the powder distribution within the pellets. Nevertheless, it is clear that IR spectroscopy is an appropriate method for identification of interlayer vacancies within phlogopitic micas.

**Acknowledgements:** The authors are grateful to I. Bauer and E.-M. Schemmert for sample preparation and to O. Appelt for her technical assistance at the electron microprobe. Helpful comments of two anonymous reviewers, by M. Andrut (Vienna), W. Heinrich (Potsdam) and M. Koch-Müller (Potsdam) on this manuscript are gratefully acknowledged.

## References

Bohlen, S.R., Peacor, D.R., Essene, E.J. (1980): Crystal chemistry of a metamorphic biotite and its significance in water barometry. *Am. Mineral.*, **65**, 55-62.

Bresson, G. & Drits, V.A. (1997): Refined relationships between chemical composition of dioctahedral fine-grained mica minerals and their infrared spectra within the OH stretching region. Part I: Identification of the OH stretching bands. *Clays Clay Minerals*, **45**, 158-169.

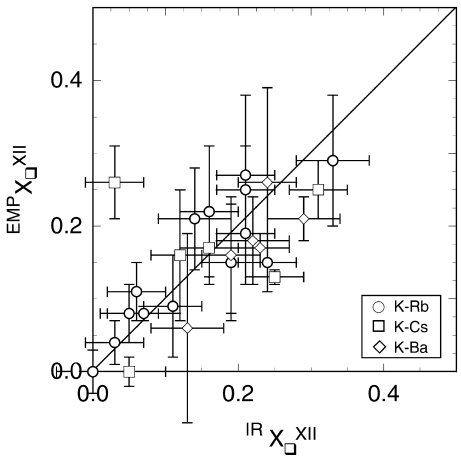


Fig. 5. Vacancy concentrations determined by EMP ($^{EMP}X_{\square}^{XII}$) *versus* vacancy concentrations determined by IR ($^{IR}X_{\square}^{XII}$). For explanation of the error bars see Table 3.

Farmer, V.C. (1974): Layer silicates. *In* Infrared spectra of minerals, Farmer, V.C. (ed.). Mineral Soc., London, 331-360.

Fernandez, M., Serratosa, J.M., Johns, W.D. (1970): Pertubation of the stretching vibration of OH groups in phyllosilicates by the interlayer cations. Proc. Reunion Hispano-Belga de Minerales de la Arcilla. Consejo Superior de Investigaciones Cientificas Madrid, 164-167.

Gottschalk, M. & Andrut, M. (1998): Structural and chemical characterization of synthetic (Na,K)-richterite solid solutions by EMP, HRTEM, XRD and OH-valence vibrational spectroscopy. *Phys. Chem. Minerals*, **25**, 101-111.

Harlov, D.E., Andrut, M., Melzer, S. (2001): Characterization of $NH_4$-phlogopite $(NH_4)(Mg_3)[AlSi_3O_{10}](OH)_2$ and $ND_4$-phlogopite $(ND_4)(Mg_3)[AlSi_3O_{10}](OH)_2$ using IR spectroscopy and Rietveld refinement of XRD spectra. *Phys. Chem. Minerals*, **28**, 77-86.

Larson, A.C. & Von Dreele, R.B. (1987): Generalized structure analysis system. Los Alamos National Laboratory Rep. No. LA-UR-86-748.

Libowitzky, E. & Rossman, G.R. (1997): An IR calibration for water in minerals. *Am. Mineral.*, **82**, 1111-1115.

Melzer, S. & Wunder, B. (2001): K-Rb-Cs-partitioning between phlogopite and fluid: experiments and consequences on the LILE-signatures of island arc basalts. *Lithos*, **59**, 69-90.

Pouchou, J.L. & Pichoir, F. (1984): Un nouveau modèle de calcul pour la microanalyse quantitative par spectrométrie de rayons X. *Rech. Aérosp.*, **3**, 167-192.

Rayner, J.H. (1974): The crystal structure of phlogopite by neutron diffraction. *Mineral. Mag.*, **39**, 850-856.

Robert, J.-L. & Kodama, H. (1988): Generalization of the correlations between hydroxyl-stretching wavenumbers and composition of micas in the system $K_2O$-MgO-$Al_2O_3$-$SiO_2$-$H_2O$: a single model for trioctahedral and dioctahedral micas. *Am. J. Sci.*, **288**, 192-212.

Robert, J.-L., Volfinger, M., Barrandon, J.-N., Basutçu, M. (1983): Lithium in the interlayer space of synthetic trioctahedral micas. *Chemical Geol.*, **40**, 337-351.

Sartori, F., Franzini, M., Merlino, S. (1973): Crystal structure of a $2M_2$ lepidolite. *Acta. Cryst.*, **B29**, 573-578.

Tateyama, H., Shimoda, S., Sudo, T. (1976): Infrared absorption spectra of synthetic Al-free magnesium micas. *N. Jb. Mineral. Mh.*, **1976**, 128-140.

Vedder, W. (1964): Correlations between infrared spectrum and chemical composition of mica. *Am. Mineral.*, **49**, 736-768.

Velde, B. (1983): Infrared OH-stretch bands in potassic micas, talcs and saponites; influence of electronic configuration and site of charge compensation. *Am. Mineral.*, **68**, 1169-1173.

Wunder, B., Baronnet, A., Schreyer, W. (1997): Ab-initio synthesis and TEM confirmation of antigorite in the system MgO-$SiO_2$-$H_2O$. *Am. Mineral.*, **82**, 760-764.

*Received 16 November 2001*
*Modified version received 13 March 2002*
*Accepted 24 May 2002*